Journal of Magnetic Resonance **141,** 291–300 (1999)
Article ID jmre.1999.1887, available online at http://www.idealibrary.com on IDEAL®

Non-Kramers ENDOR and ESEEM of the $S = 2$ Ferrous Ion of $[Fe(II)EDTA]^{2-}$

Ruitian Song, Peter E. Doan, Ryszard J. Gurbiel, Bradley E. Sturgeon, and Brian M. Hoffman

Department of Chemistry, Northwestern University, Evanston, Illinois 60208

Received April 26, 1999; revised July 27, 1999

We report here the first non-Kramers (NK) ESEEM and ENDOR study of a *mono*nuclear NK center, presenting extensive parallel-mode ESEEM *and* ENDOR measurements on the $S_t = 2$ ferrous center of [Fe(II)ethylenediamine-*N*,*N*,*N*′,*N*′-tetraacetato]$^{2-}$; [Fe(II)EDTA)]$^{2-}$. The results disclose an anomalous equivalence of the experimental patterns produced by the two techniques. A simple theoretical treatment of the frequency-domain patterns expected for NK-ESEEM and NK-ENDOR rationalizes this correspondence and further suggests that the very observation of NK-ENDOR is the result of an unprecedentedly large hyperfine enhancement effect. The mixed nitrogen–carboxylato oxygen coordination of [Fe(II)EDTA]$^{2-}$ models that of the protein-bound diiron centers, although with a higher coordination number. Analysis of the NK-ESEEM measurements yields the quadrupole parameters for the ^{14}N ligands of [Fe(II)EDTA]$^{2-}$, $K = 1.16(1)$ MHz, $0 \leq \eta \leq 0.05$, and the analysis indicates that the electronic zero-field splitting tetragonal axis lies along the N–N direction.

Key Words: **ENDOR; electron-nuclear double resonance; ESEEM; electron spin-echo envelope modulation; non-Kramers; [Fe(II)EDTA]$^{2-}$.**

Integer-spin systems with $S > 1$ are typically difficult to study by paramagnetic resonance techniques, but they sometimes exhibit a ground state "non-Kramers (NK) doublet" which is rendered EPR active by a zero-field splitting whose energy, $h\Delta$, is comparable to the microwave quantum, $h\nu_e$ (*1–3*). For example, protein-bound, carboxylate-bridged diiron(II) centers frequently display the characteristic EPR spectrum associated with a ground-state non-Kramers doublet, and NK-EPR measurements have become an important tool in the study of metallobiomolecules (*4, 5*). Nonetheless, there had been *no* reports of ENDOR or ESEEM on *any* non-Kramers doublet system until we first applied these techniques to the doublets of diferrous methane monoxygenase hydroxylases ($MMOH_{red}$) and azidohemerythrin (N_3Hr_{red}) (*6*). Subsequently we reported an analysis of ESEEM from a NK doublet of an integer-spin system (*7*) and followed this by an extensive study of the NK ground state of the pivotal diiron(II) form of the oxygen-activating nonheme diiron enzymes (*8*).

Our experiments to date have focused on the parallel-mode three-pulse, stimulated-echo NK-ESEEM spectra of the ferromagnetically coupled, *di*ferrous clusters, and the theoretical analysis created to describe the frequencies and intensities of the ^{14}N peaks appears to work well in these particular systems. We report here the first study of a *mono*nuclear NK center, presenting extensive parallel-mode ESEEM *and* ENDOR measurements on the $S_t = 2$ ferrous center of Fe(II)ethylenediamine-*N*,*N*,*N*′,*N*′-tetraacetato; [Fe(II)EDTA)]$^{2-}$. In this complex the ferrous ion has a seven-coordinate structure close to a monocapped trigonal prism with H_2O as the cap and the Fe–OH_2 bond as an approximate C_2 symmetry axis for the coordination sphere (Fig. 1). The mixed nitrogen–carboxylato oxygen coordination of [Fe(II)EDTA]$^{2-}$ (*9*) models that in the protein-bound diiron centers (*10, 11*), although with a higher coordination number.

The study of simple iron complexes with NK doublets as ground states is of particular advantage for the development of paramagnetic resonance techniques and for testing theories because such complexes can be prepared in much higher concentrations than the protein samples. This permits ready collection of extended data sets over a wide range of instrumental parameters, which is necessary for correlation with theory. The results for [Fe(II)EDTA]$^{2-}$ are compared with extensions of the theory that provide formulae which describe frequency-domain three-pulse ESEEM spectra and which explain the surprising finding that the NK-ESEEM and NK-ENDOR patterns are virtually indistinguishable in shape.

MATERIAL AND METHODS

A solution of [Fe(II)EDTA]$^{2-}$ was prepared by adding $Fe(II)Cl_2$ (to ~5 mM) to a solution of excess Na_4EDTA in degassed 1/1 ethylene glycol/deionized water. X-band ESEEM and ENDOR spectra were acquired at 2 K with a laboratory-built spectrometer described elsewhere (*12*). As before (*6, 8*), a static field, B_0, oriented parallel to the B_1 field, was produced by a pair of Helmholtz coils mounted around the tail of a liquid helium immersion dewar. The magnetic field was measured using a F. W. Bell Model 4048 Gaussmeter. ESEEM time waves were collected using a standard three-pulse stimulated echo sequence (*13–15*). The frequency-domain spectra were

1090-7807/99 $30.00

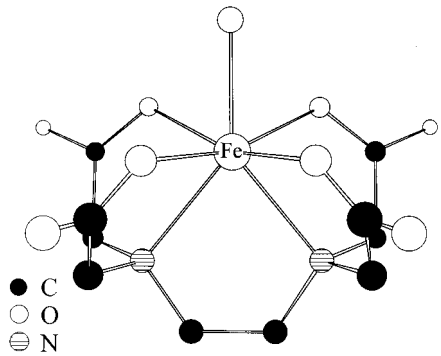

FIG. 1. Structure of the $[Fe(II)EDTA]^{2-}$ ion as determined by Miyoshi and co-workers (*9*).

produced using the deadtime reconstruction method of Mims before Fourier transformation (*16*).

RESULTS

Theory

This section generates theoretical NK-ESEEM and NK-ENDOR envelopes for comparison with the experiments reported here first. It begins with a summary of essential aspects of the theoretical framework for understanding NK-ESEEM and ENDOR (*7, 8*).

Griffith (*17*) rigorously showed that EPR measurements on an isolated NK doublet can be described in terms of a fictitious electron spin $S = \frac{1}{2}$ that experiences a zero-field splitting by an "internal field," energy $h\Delta$, as well as by a Zeeman interaction proportional to the projection of the applied field along a real-space axis, denoted the z axis. The combined action of the applied and internal fields splits the NK doublet by a frequency ν_e (Eq. [1]),

$$\nu_e = \left[\Delta^2 + \left(\frac{\tilde{g}_\parallel \beta B_z}{h} \right)^2 \right]^{1/2}; \quad B_z = B_0 \cos\theta \equiv B_0 z, \quad [1]$$

where θ is the angle between the z axis and the applied field, $\mathbf{B}_0$, $z = \cos\theta$ ($0 \leq \theta \leq 90°$), and the effective g value along this axis is, $\tilde{g}_\parallel = (2nS_t)g_\parallel$, where, S_t is the single-ion spin and n is the number of exchange-coupled ions; (for $[Fe(II)EDTA]^{2-}$, $S_t = 2$ and $n = 1$). In general, the splitting Δ for a NK doublet is distributed. As a result, for a frozen solution subjected to any applied field, B_0, the resonance condition will be satisfied with equal probability by molecules of every orientation, because for each θ there are molecules whose value of Δ is such that ν_e equals the microwave frequency, ν_m.

For $I = 1$, the nuclear-transition frequencies measured by ESEEM and ENDOR can be described in terms of a spin Hamiltonian, $\hat{H}_{nuc}(m_S)$, Eq. [2], expressed in the coordinate frame that diagonalizes the nuclear quadrupole interaction term. The P_i in Eq. [2] are the principal values of the nuclear quadrupole interaction

$$\hat{H}_{nuc}(m_s) = m_s \tilde{A}_{eff} \sum_i \cos\alpha_i \hat{I}_i + \sum_i P_i \hat{I}_i^2 \quad [2]$$

tensor. In addition to the quadrupole interaction, $\hat{H}_{nuc}(m_s)$ includes a hyperfine term whose *effective* hyperfine coupling, $\tilde{A}_{eff}$, depends on the z-component of the field, Eq. [3], on the projection of the hyperfine interaction along the z axis axis, $A_\parallel$, and parametrically on m_s; the ($\cos\alpha_i$) in Eq. [2] are the direction cosines of the cluster z axis relative to the quadrupole axes.

$$\tilde{A}_{eff} = \tilde{A}_\parallel \left(\frac{\tilde{g}_\parallel \beta B_z}{h\nu_e} \right); \quad \tilde{A}_\parallel = (2S_t) A_\parallel. \quad [3]$$

This Hamiltonian is appropriate for experiments, such as those reported here, which are performed at sufficiently low applied fields that the nuclear–Zeeman interaction can be ignored. $\hat{H}_{nuc}(m_s)$ is field-dependent, even without the nuclear–Zeeman term, because of the field dependence of $\tilde{A}_{eff}$. The quadrupole tensor is traceless, $P_1 + P_2 + P_3 = 0$, and we choose the three principal components so that $P_1 < P_2 < P_3$; typically, for ^{14}N, the P_1 component will be the largest in magnitude. Transitions among the three nuclear levels defined by the quadrupole interaction for $I = 1$ are the three pure nuclear–quadrupole frequencies, defined as ($\bar{\nu}_0 < \bar{\nu}_- < \bar{\nu}_+$), and given by Eq. [4].

$$\begin{aligned} \bar{\nu}_+ &= \bar{\nu}_{13} = P_3 - P_1 \\ \bar{\nu}_- &= \bar{\nu}_{12} = P_2 - P_1 \\ \bar{\nu}_0 &= \bar{\nu}_{23} = P_3 - P_2. \end{aligned} \quad [4]$$

The quadrupole tensor also is commonly parametrized in terms of $K = |P_1|/2 = e^2qQ/4$ (usual symbols) and $\eta = (P_3 - P_2)/|P_1|$.

The Hamiltonian $\hat{H}_{nuc}(m_s)$ can be diagonalized for $I = 1$ by use of published equations (Eqs. [10] and [11] of Ref. (*18*)). The resulting energies (but *not* the wavefunctions) are the same in both electron-spin ($m_s = \pm\frac{1}{2}$) manifolds because the nuclear–Zeeman term has been ignored, and thus the coupled NK-electron-spin, nuclear-spin system shows three doubly degenerate ENDOR frequencies for a given orientation. These frequencies, which depend on B_z through $\tilde{A}_{eff}$ (Eq. [3]), are denoted (ν_+, ν_-, ν_0) because, as $B_z \to 0$, they evolve into the pure quadrupole frequencies, ($\bar{\nu}_+$, $\bar{\nu}_-$, $\bar{\nu}_0$). The behavior of the exact solutions is exhibited explicitly in the field-dependent shifts of the transition frequencies, $\delta\nu_{ij}$, as calculated to second order in the hyperfine interaction. When, $\eta > 0$, these are given by Eq. [5] (*7*),

$$\delta\nu_{ij} = \nu_{ij} - \bar{\nu}_{ij} = \left[\sigma_{ij}\left(\frac{\tilde{A}_\parallel \tilde{g}_\parallel \beta}{h\nu_e}\right)^2 B_o^2\right]\cos^2\theta \quad (\eta > 0)$$
$$= \delta\nu_{ij}^{\max} z^2. \qquad [5]$$

For use below, we further define the extremal frequency of a transition, $\nu_{ij}^{\max} = \bar{\nu}_{ij} + \delta\nu_{ij}^{\max}$. As $\eta \to 0$, two of the nuclear levels become degenerate and the (ν_+, ν_-) transitions shift linearly with applied field, with transition frequencies that have a first-order, linear dependence on applied field,

$$\delta\nu_{ij} = \left[\frac{m_{ij}}{2}\left(\frac{\tilde{A}_\parallel g_\parallel \beta}{h\nu_e}\right)\cos\alpha_3 B_0\right]\cos\theta \quad (\eta \to 0)$$
$$= \delta\nu_{ij}^{\max} z. \qquad [5a]$$

Here, m_+ $(i, j = 1, 3) = +1$, m_- $(i, j = 1, 2) = -1$, and m_0 $(i, j = 2, 3) = +2$. This equation is exact for all fields when B_0 and the z axis are parallel ($\cos\alpha_3 = 1$), but is valid only for low fields for an arbitrary field orientation. Because of the 1:1 correspondence between orientation (z) and frequency shift ($\delta\nu_{ij}$) the latter can be parametrized in terms of the extremal shift at the applied field, $\delta\nu_{ij}^{\max}$ and a normalized frequency shift,

$$\delta \equiv \frac{\delta\nu_{ij}}{\delta\nu_{ij}^{\max}} = z^2 \quad (\eta > 0)$$
$$= z \quad (\eta \to 0). \qquad [5b]$$

The $\delta\nu_{ij}^{\max}$ depend both on the pure quadrupole frequencies and on the orientation of the cluster z axis with respect to the quadrupole frame, denoted as $\cos(\alpha_i)$ (the coefficients, σ_{ij}, for the case $\eta > 0$ are given in Eq. [21b] of Ref. (*8*)). For ν_- $(i, j = 1, 2)$ and ν_0 $(i, j = 2, 3)$ the shifts can be either positive or negative, but that for ν_+ $(i, j = 1, 3)$ is necessarily positive. This perturbation treatment for $I = 1$ nuclei, which is the basis for the analytical forms developed in the following section, has been confirmed by exact calculations.

When considering hyperfine coupling to a nucleus of $I = \frac{1}{2}$, there is no quadrupole interaction and one cannot ignore the nuclear–Zeeman interaction even at low field. The exact values for the orientation-dependent nuclear transition frequencies, $\nu_\pm(\theta)$, which vary linearly with B_0 ($\pm$ refers to $m_s = \pm\frac{1}{2}$), are (*7*)

$$h\nu_\pm(\theta) = \left[\left(\pm\frac{\tilde{A}_\parallel}{2}\frac{\tilde{g}_\parallel\beta}{h\nu_e} + g_n\beta_n\right)^2\cos^2\theta + (g_n\beta_n)^2\sin^2\theta\right]^{1/2} B_0$$
$$= \left[g_n\left\{\left(\pm\frac{1}{2}\frac{\tilde{A}_\parallel}{h\nu_e}\frac{\tilde{g}_\parallel\beta}{g_n\beta_n} + 1\right)^2\cos^2\theta + \sin^2\theta\right\}^{1/2}\right]\beta_n B_0$$
$$\equiv \tilde{g}_{n\pm}(\theta)\beta_n B_0. \qquad [6]$$

For the limiting case, $\theta = 0$, this equation predicts a spectrum with the same general form as seen in conventional ENDOR spectra. For $\tilde{A}_{\text{eff}}/\nu_n < 1$ there is a pair of transitions centered at ν_n and split by $\tilde{A}_{\text{eff}}$, while for the reverse inequality there is a pair split by twice the Larmor frequency, centered at $\tilde{A}_{\text{eff}}/2$; for the limit, $\theta = \pi/2$, there is only a transition at the Larmor frequency.

NK-ESEEM, ENDOR envelopes. As a result of the distribution in Δ, at field B_0 the frequencies for each nuclear transition will exhibit contributions from all orientations and hence the full range of frequencies (frequency shifts) associated with $0 \le B_z \le B_0$. To describe an ESEEM or ENDOR experiment, it is necessary to calculate the resultant lineshape in the frequency domain.

NK-ESEEM; I = 1. The electron-spin echo (ESE) modulation for a NK doublet vanishes at $B_0 = 0$, but is predicted to increase quadratically with the applied field (*7*). The ESEEM intensity for a particular frequency/orientation is given by the product of the modulation *fraction* and the contribution to the ESE *intensity* from that frequency/orientation. In the perturbation treatment, the *fractional* modulation for each of the $\{i - j\}$ transitions associated with a particular orientation (z) is given by a modulation depth parameter of the form, $I_e(z) \propto b^2(z) \propto z^2$. Upon change of variables to the normalized shift parameter, δ, the "statistical" lineshape, $I_e(\delta)$, is the product of the square of a modulation-depth parameter, $b^2(\delta) \propto \delta$, and the quantity, $dz(\delta)/d\delta$, which comes from the transformation between the variables z and δ (*8*),

$$I_e(\delta) \propto b^2(\delta)\frac{dz}{d\delta}(\delta)$$
$$\propto \delta^{1/2} \quad (\eta > 0)$$
$$\propto \delta^2 \quad (\eta \to 0). \qquad [7]$$

To describe the NK-ESE intensity we recall that in a parallel-mode experiment, where B_1 is the pulsed microwave field applied parallel to the static field ($B_1 \| B_0$), the on-resonance electron-spin "turning angle," Θ_p, during an applied microwave pulse of duration, t_p, is strongly orientation-dependent (*7*),

$$\Theta_p(z) = \left[\left(\tilde{g}_\parallel\beta\frac{B_1}{2}\sin\xi\right)t_p\right]z. \qquad [8]$$

This behavior is quite unlike that for typical Kramers centers. While a full discussion of the ESE intensity will be presented

in a future report, in the limit of microwave pulses with small turning angle (small ($B_1 t_p$)), the contribution to the ESE amplitude from a particular orientation is proportional to $\sin^3\Theta_p(z)$ (*14*), which can be expanded for small z,

$$\begin{aligned} am(z) &\propto \sin^3\Theta_p(z) \propto \Theta_p(z)^3 \propto z^3 \\ am(\delta) &\propto \delta^{3/2} \quad (\eta > 0) \\ &\propto \delta^3 \quad (\eta \rightarrow 0). \end{aligned} \tag{9}$$

This leads to a common form for the envelope, denoted $Ies(\delta)$, for each $\{i - j\}$ transition in a frequency-domain ESEEM spectrum,

$$\begin{aligned} Ies(\delta) &\propto am(\delta) I_e(\delta) \propto \delta^2 \quad (\eta > 0) \\ &\propto \delta^5 \quad (\eta \rightarrow 0). \end{aligned} \tag{10}$$

To finally describe the actual ESEEM lineshape requires the inclusion of the "suppression" term, in which the ESEEM frequencies associated with one m_S manifold are suppressed by those associated with the other (*14*). The equality of the ENDOR frequencies in the two NK manifolds means that each frequency is suppressed by itself. Previously (*8*), in writing this term we ignored the hyperfine shifts (Eq. [5]) compared to the pure quadrupole frequencies (Eq. [4]); the full suppression term can be written in current notation as

$$supes(\nu_{ij}(\delta)) = (1 - \cos(2\pi\nu_{ij}(\delta)\tau)), \tag{11}$$

leading to the prediction then a NK-ESEEM peak will have the form

$$Ses_{ij}(\delta) \propto supes(\nu_{ij}(\delta)) Ies(\delta). \tag{12}$$

Convolution of this function over a component lineshape then yields the final prediction for an experimentally observed peak. The function, Eq. [12], and the final peak shape obtained by convolution are illustrated in the inset to Fig. 4.

NK-ESEEM; $I = \frac{1}{2}$. Recall that we presented an exact formula for the orientation-dependent modulation-depth parameter for $I = \frac{1}{2}$ (*7*). Its functional form is such that the modulation vanishes for $\theta = 0$ and $\pi/2$, maximizing at an intermediate angle. Of central interest to our experiments, while there is again no modulation at zero applied field, at nonzero fields the fractional modulation depth, integrated over all orientations, is predicted to be independent of the applied field. However, because the observed modulation includes the suppression term (Eq. [11]) as a factor, the modulation depth will have a strong dependence on the applied field (and on τ) because the ENDOR frequency that appears in the suppression term increases linearly with the field (Eq. [6]). This, therefore, contrasts with the case of $I = 1$, where the nuclear frequencies are dominated by the field-independent quadrupolar contribution, and an applied field causes relatively small *shifts* in frequency. For $I = \frac{1}{2}$ at low fields and fixed value of τ, expansion of the trigonometric function in the suppression term leads to the prediction that the modulation depth for $I = \frac{1}{2}$ should increase quadratically with the applied field for small fields.

NK-ENDOR; $I = 1$. The corresponding lineshape for a NK-ENDOR spectrum can be obtained by an analogous procedure. Namely, the absolute ENDOR intensity at a frequency offset δ for transition $\{i - j\}$ should be proportional to the product of the RF field (B_2)-induced nuclear transition probability, $enh^2(\delta)$, and the ESE amplitude. Following the procedures used for Kramers systems (*19*), we have calculated the NK-ENDOR transition probability using nuclear wavefunctions corrected to first order in the hyperfine interaction. As with a Kramers system, the transition probability is proportional to a "hyperfine-enhancement factor" which deviates from unity through the off-diagonal contributions of the hyperfine coupling. For a NK system this factor is strongly dependent on orientation and thus on the frequency shift, but nonetheless for comparison it can be cast in the form of a Kramers system at X band,

$$enh^2(z) \propto (1 + m_S a(z)/\nu_{NX})^2, \tag{13}$$

where the first term is from direct nuclear transitions. The second, which reflects the enhancement, involves a frequency-shift-dependent hyperfine parameter with an approximate value

$$a_{ij}(z) \simeq [n(2S_t)^2 A_{\|} \cos\alpha_{ij}] z. \tag{13a}$$

Here, ν_{NX} is the nuclear Larmor frequency at X band and $n = 1$ for $[Fe(II)EDTA]^{2-}$. As we discuss below, one can neglect the contribution from direct transitions, in which case the ENDOR transition probability, and thus the *fractional* ENDOR effect, has the dependence

$$enh^2(z) \propto z^2. \tag{13b}$$

But this is the same form as the ESEEM modulation-depth parameter, $b^2(z)$, which leads to the statistical lineshape, $I_e(\delta)$ (Eq. [7]). The result is that the *fractional* ENDOR-induced change in the ESE amplitude, $I_E(\delta)$, is predicted to have the same statistical lineshape for each transition as the fractional ESEEM modulation:

$$\begin{aligned} I_E(\delta) &\propto I_e(\delta) \equiv I(\delta) \propto \delta^{1/2} \quad (\eta > 0) \\ &\propto \delta^2 \quad (\eta \rightarrow 0). \end{aligned} \tag{14}$$

The observed ENDOR response, denoted $Ien(\delta)$, then, is the echo amplitude multiplied by the fractional ENDOR effect, as given above. Taking the small-turning-angle limit ($\delta^{3/2}$) for the

former, each peak in a NK-ENDOR spectrum has the envelope shape

$$Ien(\delta) \propto am(\delta)I(\delta) \propto \delta^2 \quad (\eta > 0)$$
$$\propto \delta^5 \quad (\eta \to 0). \qquad [15]$$

This treatment thus predicts that frequency-domain NK-ESEEM and NK-ENDOR spectra exhibit the *same* envelope function. The observed Mims ENDOR effect further involves a suppression term, which is a function of the hyperfine coupling. If we denote this term as $supen_{ij}(\delta)$, then the NK-ENDOR signal for the $\{i - j\}$ transition would have the form

$$Sen_{ij}(\delta) \propto supen_{ij}(\delta)Ien(\delta). \qquad [16]$$

We defer the discussion of $supen_{ij}$ until the presentation of the experimental data.

NK-ESEEM Measurements

For comparison, we recall that in an X-band CW spectrometer the integer-spin diferrous centers commonly give a broad, NK-EPR signal with intensity that extends from zero applied field with an apparent g-value of $g \sim 16$ (5). In a pulsed spectrometer, the diferrous centers give a strong spin echo at zero applied field but the phase memory shortens with increasing field such that an echo is undetectable at fields above ~50 G. The echo shows no modulation at zero applied field, but modulation rapidly appears with fields of a few Gauss, a curious phenomenon explained by the field-dependent effective hyperfine coupling.

The $S_t = 2$ $[Fe(II)EDTA]^{2-}$ ion also shows a NK-EPR signal. It too extends from the zero applied field, with a shape that indicates the splitting Δ is distributed, but with an apparent $g \sim 8$ as expected for a single $S = 2$ ferrous ion with a negative zero-field splitting ($D < 0$). The existence of this signal indicates that the major distortion of the ferrous-ion ^5E state is an axial elongation that produces the negative zero-field splitting and a ground state in which the lowest energy d-orbital is d_{x2-y2}. As with the diiron centers, in zero applied field there is a readily detectable X-band ESE with no observable modulation (Fig. 2). The echo, which decreases in intensity with field, is observable up to ~200 G for relatively short τ values (<200 ns).[1] Modulation of the time waves appears at fields of a few Gauss (Fig. 2). There is a strongly field-dependent, unresolved low-frequency component at the proton Larmor frequency. The intensity of this modulation, measured as a fraction of the echo, increases strongly with field, with the increase roughly following the quadratic dependence noted above.

The time waves also exhibit clear modulation with higher frequency components, and frequency-domain spectra (Fig. 3A; $\tau = 100$ ns) display two peaks in the vicinity of 3.5 MHz whose positions vary with the applied field. We assign these to the (ν_-, ν_+) transitions among the $I = 1$ nuclear sublevels of the coordinating ^{14}N ligand atoms of $[Fe(II)EDTA]^{2-}$. Up to fields of ~45 G the modulation, considered a percentage of the echo intensity, increases in strength with the applied field; at higher fields the modulation percentage decreases, presumably because of shortening phase memory. As τ is raised the modulation also weakens, and it is difficult to detect for $\tau \geq 300$ ns. To low frequency in each spectrum (not shown) there is a strong feature from protons that is centered at the proton Larmor frequency; no additional ^{14}N transition has been observed.

Given that EDTA provides two nitrogen ligands to the ferrous ion, one might propose that the two peaks in the vicinity of 3.5 MHz are the distinct ν_+ transitions of two

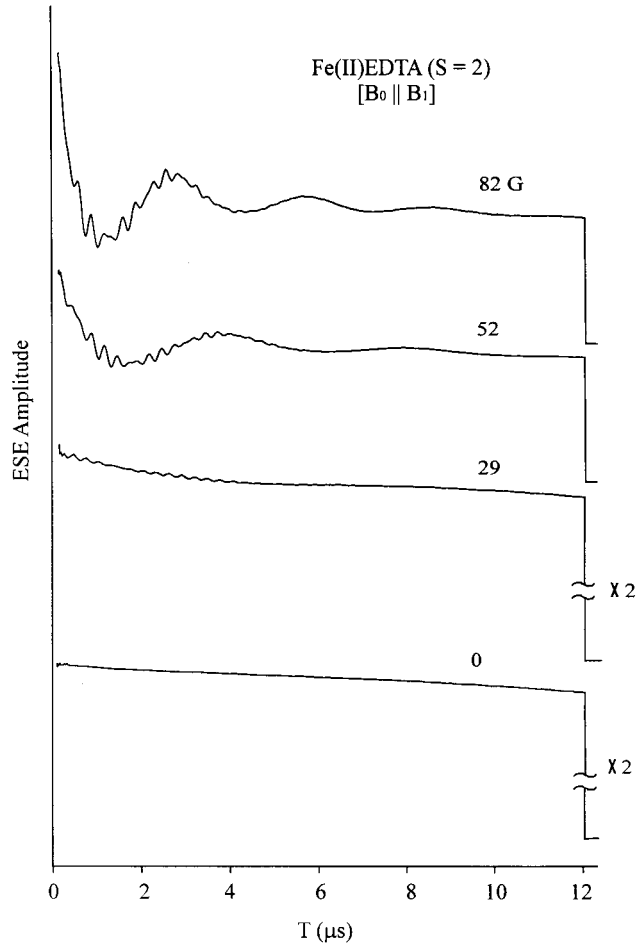

FIG. 2. Field dependence of fractional three-pulse NK-ESEEM time waves of $[Fe(II)EDTA]^{2-}$. In these traces the absolute ESEEM signal has been divided by the echo intensity. The traces for 0 and 29 G have been multipled by 2 to show the weak modulation. Conditions: B_0 parallel to the mw field B_1; mw frequency = 9.50 GHz; pulse width $t_p = 16$ ns; $\tau = 100$ ns; increment in T is 24 ns; samples/point = 40; repetition time = 10 ms; temperature, 2 K.

[1] The behavior in the perpendicular mode is quite different, with an ESE being detectable to ~2000 G.

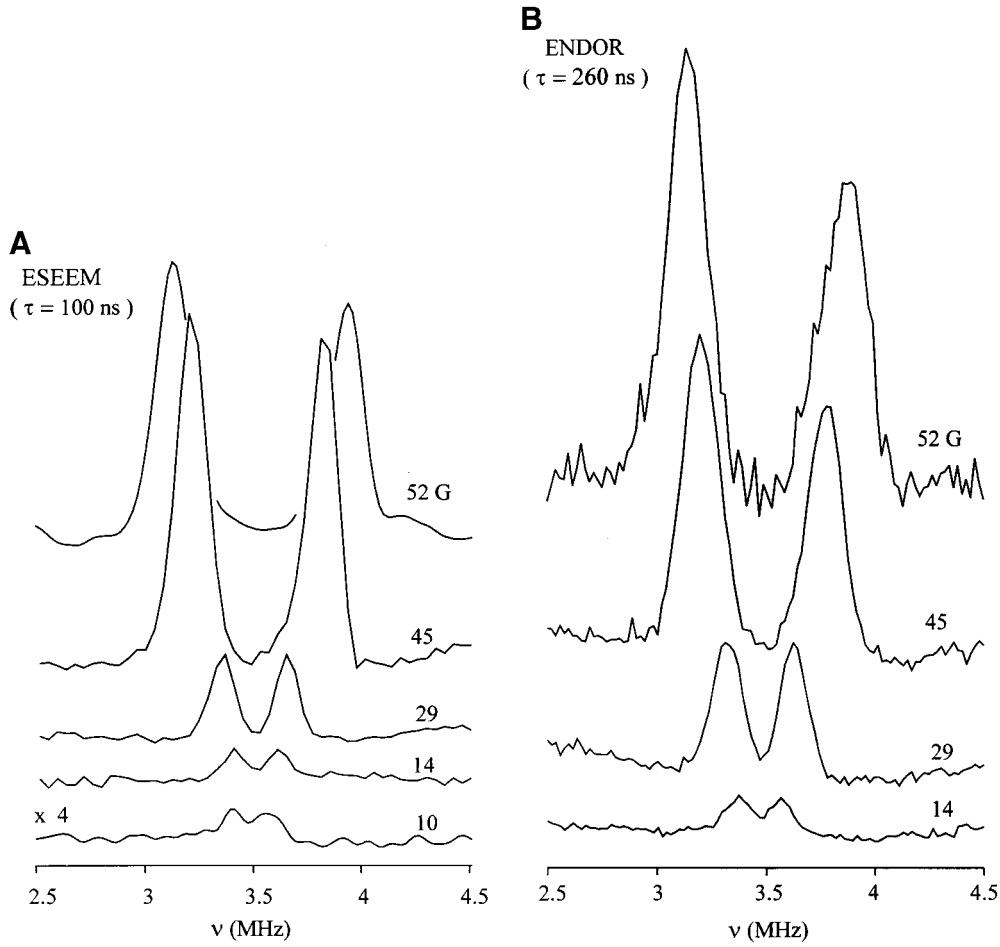

FIG. 3. (A) Field dependence of three-pulse fractional NK-ESEEM of $[Fe(II)EDTA]^{2-}$ in the frequency domain. Conditions: As in Fig. 2; Fourier transform procedure is described under Material and Methods. (B) Field dependence of fractional Mims ENDOR of $[Fe(II)EDTA]^{2-}$ Conditions: As in Fig. 2, with the additional parameters: $\tau = 260$ ns; $T = 18.62$ μs; RF power, 250 W, 10 μs duration.

slightly different nitrogens, with ν_- (and ν_0, which would come at low frequency) not observed because of low intensities. However, general considerations (*7*) show that ν_+ must shift to higher frequency as B_0 increases from zero, while one of the observed peaks shifts to lower frequency, so this interpretation can be dismissed. Instead we assign these features to the ν_+ and ν_- ^{14}N NQR peaks of the two bound ^{14}N which are equivalent and hence have the same transition frequencies.

If the quadrupole asymmetry parameter, η, were relatively large, as for Fe-bound histidines, it would be straightforward to obtain the pure-quadrupole frequencies (Eq. [4]) for $[Fe(II)EDTA]^{2-}$ by extrapolation of the ν_+ and ν_- ^{14}N peaks to zero field; these peaks would shift quadratically with field for small B_0 and thus would reach a well-defined limiting value (Eq. [5]) (*8*). However, for $[Fe(II)EDTA]^{2-}$ we find that the ν_+ and ν_- transitions diverge roughly linearly with field above ~10 G. Because the modulation vanishes as $B_0 \rightarrow 0$, it is not possible to unambiguously distinguish between the quadratic shift as $B_0 \rightarrow 0$, expected when $\eta \rightarrow 0$, and a linear divergence from a common zero-field frequency, which is expected when $\eta \rightarrow 0$. As a result, it is necessary to use the theory presented above to model the experimental spectra in order to derive spin Hamiltonian parameters. Such modeling is necessary because at nonzero fields the transition frequencies calculated theoretically, and in particular the extremal NK-ESEEM frequencies, the ν_{ij}^{max}, differ slightly from the measurable peak frequencies, denoted ν_{ij}^{obs}.

The above analysis indicates that NK-ESEEM spectra in the low-turning-angle limit should be described by convolution of an appropriate component lineshape over the envelope function, $Ses_{ij}(\delta)$ (Eq. [12]). To match experiment to theory at a particular field, we forced the peak frequencies of a calculated spectrum, ν_{ij}^{obs}, to match those measured for the experimental one and report the theoretical values of the ν_{ij}^{max} given by the calculation (Fig. 4). The experimental ν_{ij}^{obs}, and hence the ν_{ij}^{max}, increase roughly linearly with the applied field (Fig. 4), and therefore the spectra are modeled with Eqs. [10] ($\eta \rightarrow 0$) through [12], which are appropriate for such a linear variation (and whose use does *not* require the low-field condition utilized in the derivation). This calculation is illustrated in the inset to

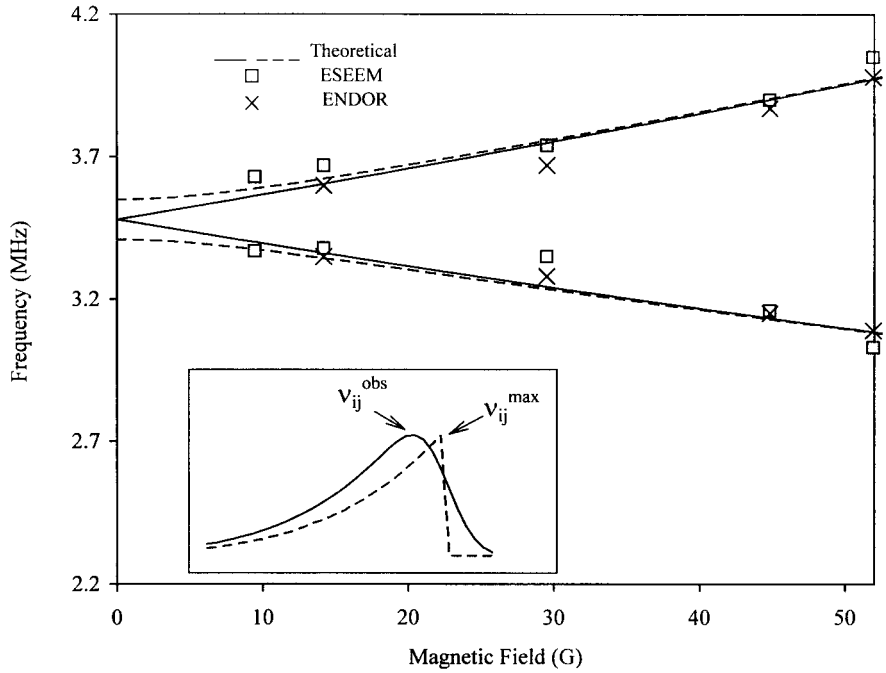

FIG. 4. Field dependence of the NK-ESEEM (□) and NK-ENDOR (×) frequencies, ν_{ij}^{max}, determined from the experimental frequency-domain spectra by modeling them as discussed in the text. This is illustrated in the inset, the envelope function, Eq. [12], $\eta \rightarrow 0$, (dashed line) along with the calculated spectrum (solid line) obtained by convolution; here, the maximum heights of the envelope function and calculated spectrum are normalized. Curves of ν_{ij}^{max} obtained by two optimized calculations in which the exact Muha expressions were used to calculate the ν_{ij}^{max} for (ν_+, ν_-) are included. The solid line uses $\eta = 0$ while the dashed line uses $\eta = 0.05$; the other parameters are $K = 1.16$ MHz, $A_\parallel = 18$ MHz, and $\alpha_3 = 53°$.

Fig. 4, which presents a plot of the envelope function (Eq. [12]), as well as the peak obtained from it by convolution. As is clearly shown in Fig. 5, the observed spectra are well reproduced in this way, even though the experiments do not reach the low-turning-angle limit employed in the derivation. In fact, the detailed form of the envelope function is not critical. Quite similar shapes, and essentially the same $\delta\nu_{ij}^{max}$, are obtained by employing spectra calculated with the equations based on a quadratic relation of field and frequency or by employing the statistical lineshape, $I_e(\delta)$, derived from exact calculations of the frequencies and wavefunctions. Moreover, direct calculations under way show that relaxation of the small-turning-angle approximation has little effect until the turning angle for $z = 1$ becomes greater than $\sim\pi/2$.

Figure 4 plots the field dependence of the ν_{ij}^{max} derived from the experimentally observed peaks, along with the results of two calculations of (ν_+^{max}, ν_-^{max}), each optimized to reproduce the experiments. The calculations employed the exact frequency expressions of Muha (*18*). Although the experimental frequencies shift approximately linearly with field, as predicted by the perturbation treatment of Eq. [5a] ($\eta \rightarrow 0$), this treatment is not valid even for the small fields of the plot, up to 60 G. For one of the calculations it is assumed that the two frequencies approach the common zero-field limit, $\bar{\nu}_- = \bar{\nu}_+ = 3.48(1)$. This leads to quadrupole parameters $K = 1.16(1)$ MHz, $\eta = 0$. For most choices of the angle between the Fe–N bond (unique quadrupole axis) and the electronic z-axis, α_3, a

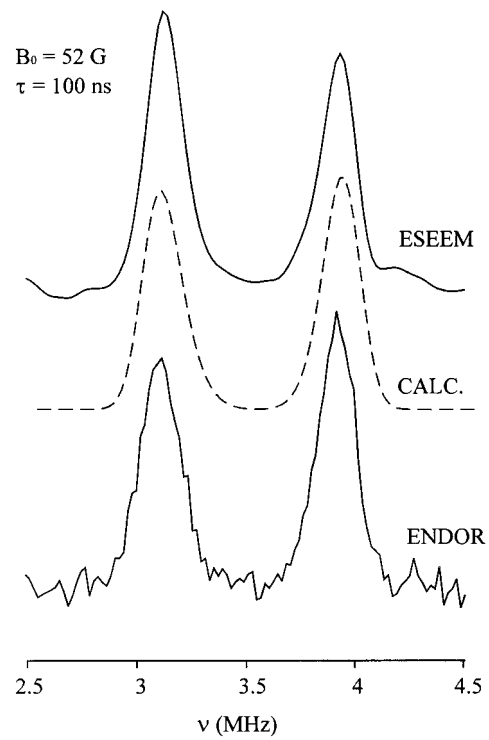

FIG. 5. Comparison of frequency-domain NK-ESEEM and ENDOR spectra of $[Fe(II)EDTA]^{2-}$ taken at 52 G and $\tau = 100$ ns. The calculated spectrum (dashed line) was obtained as described in the text and the legend to Fig. 4, with use of a linewidth of 0.1 MHz.

plot of calculated frequencies that roughly matches the experimental ones is clearly curved. However, for values of the angle between z and the Fe–N bond (unique quadrupole axis) of each of the two nitrogen ligands in the range $45° \lesssim \alpha_3 \lesssim 55°$, it was possible to choose pairs of values, $[\alpha_3, A_\parallel]$, with $A_\parallel$ varying by ± 1 MHz, that match the experiments quite well. The displayed calculation with $\eta = 0$ employed the values $\alpha_3 = 53°$ and $A_\parallel = 18$ MHz; the reason for this particular choice is clarified below. This calculation reproduces the data quite well, but the figure shows that the data can be described equally well by taking η to be nonzero. The maximum value that satisfactorily reproduces the low-field data is $\eta = 0.05$, as in the calculation presented; variations in $A_\parallel$ do not influence this observation. These two calculations thus give the limits of accuracy for the ^{14}N asymmetry parameter, $0 \leq \eta \leq 0.05$.

The quadrupole constant, $K = 1.16$ MHz, for the ^{14}N atoms of an Fe(II)-bound EDTA ligand is quite large compared to the values for the common biological N-donor ligand, histidine, for which $K \sim 0.6$ MHz (*8*), but in fact it is quite comparable to the value $K = 1.25$ MHz, which is found for the ^{14}N of trialkyl amines (*20–22*) and should apply to the trialkyl nitrogens of EDTA. The unique quadrupole axis in the free amine necessarily lies along the nitrogen lone pair and correspondingly must lie along the Fe–N coordinate bond in $[Fe(II)EDTA]^{2-}$. The small-to-zero value of η is expected for a trialkyl amine coordinated to a metal ion and is equivalent to the value $\eta = 0$ for NMe_3. Following the procedure of Roberts *et al.* (*21*), the K for $[Fe(II)EDTA]^{2-}$ can be used to estimate that each nitrogen ligand donates ~5% of an electron (~2.5% of a lone pair) to iron, a substantially smaller amount, reflecting a lesser covalency, than they found for bonding of trialkyl amine nitrogens to M = Hg^{2+}, Cd^{2+}, or Zn^{2+} ions in M(1,2-dipiperidinoethane)X_2 complexes.

Based on the approximately C_{2v} geometry of the coordination sphere, shown in Fig. 6, one would expect the electronic z-axis to lie along a symmetry axis. Examination of the structural data of Fig. 6 in light of the permissible range of values for α_3 then suggests that z lies along u (parallel to the N–N vector), which makes an angle of $\alpha_3 = 53°$ with the Fe–N bond, rather than along the Fe–O vector (t) which makes an angle of $\alpha_3 = 37°$; the result firmly rules out an assignment of z along the third axis of the fragment, normal to the plane, which would give $\alpha_3 \sim 90°$.[2]

NK-ENDOR Measurements

In our initial examination of the diiron systems (*6*), we reported Mims ENDOR spectra that looked surprisingly like those obtained in the frequency-domain ESEEM spectra. ENDOR and ESEEM experiments of Kramers systems are well known to exhibit different shapes due to the different selection rules that govern the two techniques. For example, ENDOR patterns typically accentuate the contributions from orientations associated with the hyperfine-tensor principal axes, whereas the contributions of those orientations are suppressed in the ESEEM pattern (*23*). The favorable spin properties of $[Fe(II)EDTA]^{2-}$ have given us the opportunity to compare these two types of NK measurements in greater detail.

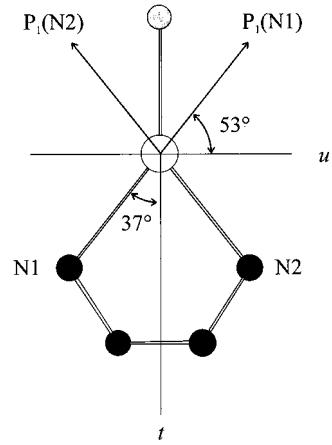

FIG. 6. Portion of $[Fe(II)EDTA]^{2-}$ structure including Fe, two ligating N atoms, and the O of water. The $[FeN_2O]$ fragment is approximately plana with a twofold axis of symmetry. There are two directions, t and u, which are discussed in the text, where it is proposed that the NK z-axis lies along u.

NK-ENDOR spectra of $[Fe(II)EDTA]^{2-}$ indeed show the same two peaks between 3 and 4 MHz as seen in the ESEEM of this sample at $B_0 = 52$ G. Just as in the ESEEM experiments, the ENDOR peaks vanish at zero field and their intensities first increase with field, then decrease as the ESE intensity decreases, becoming undetectable in the parallel mode by ~140 G.[2] The NK-ENDOR peaks also exhibit hyperfine-induced shifts from the pure-quadrupole frequencies as the applied field is increased (Fig. 3B). In fact, the 2D NK-ENDOR patterns of $[Fe(II)EDTA]^{2-}$ at $\tau = 260$ ns and fields, $B_0 \lesssim 60$ G, are essentially indistinguishable from the 2D frequency-domain NK ESEEM patterns (Figs. 3A and 3B), and the frequencies derived from the Mims NK-ENDOR experiments overlay those from the ESEEM data (Fig. 5) (*vide infra* for discussion of higher fields).

Unlike the ESEEM experiments, at present there is no theory to explain either the intensities or the lineshapes of the ENDOR peaks: if the sample had instead contained a true $S = \frac{1}{2}$ Kramers ion, the magnitude of the RF field (B_2) would have been far too low and the duration of the RF pulse too short to give a detectable ENDOR response. However, the above theoretical treatment does explain these puzzling features of NK-ENDOR spectra in terms of an unprecedentedly large RF enhancement factor, enh^2 (Eq. [13]), which reflects the RF field acting on the nuclei through its influence on the electron-spin system (*19*) which in this case is dependent on the z-component of the applied field, B_z. For example, taking $B_z \sim 50$ G and the ^{14}N spin-Hamiltonian parameters for $[Fe(II)EDTA]^{2-}$, the enhancement term has a value of $enh^2 \sim$

[2] The transition frequencies for $\eta \to 0$ necessarily vary linearly with field for $\alpha_3 \sim 0°$, but this angle is not simultaneously possible for both nitrogens.

10^3 for either value of m_S. We take this surprisingly large value to explain the ease of observing NK-ENDOR spectra.

The calculation further explains why the NK-ENDOR and NK-ESEEM spectra presented in Figs. 3 and 4 look basically the same, even though ENDOR and ESEEM spectra from Kramers systems have quite different shapes. For orientations where the NK-ENDOR enhancement term is large, it completely overwhelms the contribution from direct transitions; for orientations where the enhancement vanishes ($\cos\theta \rightarrow 0$), the echo amplitude also vanishes. As a result, one can entirely neglect the contribution from direct transitions and, as discussed above in regard to Eqs. [13b] and [14], NK-ENDOR and NK-ESEEM peaks *should* have the same envelope function, $I(\delta)$, and hence the same shapes.

Despite the fact that the results and analysis indicate that the NK-ESEEM and ENDOR are in many ways understood, at least in a semiquantitative way, there are nonetheless unresolved issues. The Mims ENDOR effect also involves a hyperfine-selective suppression factor, which depends on the product of a hyperfine parameter, $\aleph$ (for the moment undefined) and τ,

$$supen((\nu_{ij}(\delta)) = (1 - \cos(2\pi\aleph(\nu_{ij}(\delta))\tau)). \qquad [17]$$

Unlike the NK-ESEEM measurements, a broad range of τ is useable in NK-ENDOR (e.g., $100 \lesssim \tau \lesssim 1800$ ns at 14 G), and this has allowed us to explore the τ-dependent hyperfine-selection effect. As shown in Fig. 7, at fixed applied field, 45 G, the frequency shifts of the NK-ENDOR peaks decrease with increasing τ, with the peaks nearly collapsing by $\tau = 720$ ns. A model calculation shows that this effect is consistent with Eq. [17] provided that one uses the shift-dependent hyperfine factor, $\aleph = \tilde{A}_{\text{eff}}(\delta)$ in the equation. Such an effect would explain why a plot of the NK-ENDOR peak frequencies for $\tau = 260$ ns deviates from the theoretical curves of Fig. 2 for fields above ~50 G (not shown). *However*, we find that application of the Mims' heuristic analysis of hyperfine selection in Mims ENDOR (*14, 24*) to a Hamiltonian, $\hat{H}_{\text{nuc}}(m_S)$, whose eigenvalues are independent of m_S, leads to the conclusion that the appropriate value to incorporate in Eq. [17] is $\aleph \equiv 0$, in which case, $supen(\nu_{ij}) \equiv 0$. In short, such an analysis predicts that there should be no Mims NK-ENDOR effect. The resolution of this *apparent* contradiction will be addressed by combining a study of the field/τ dependences of the Mims NK-ENDOR effect with a full density-matrix treatment of this phenomenon.

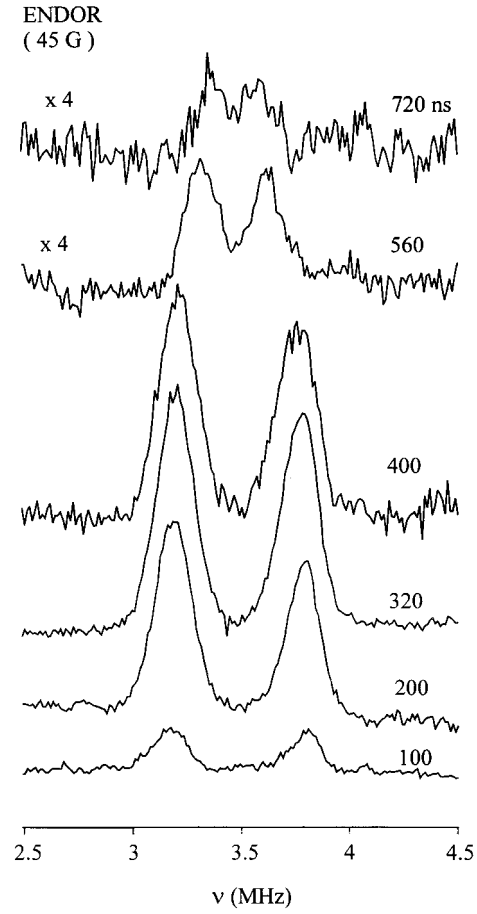

FIG. 7. The τ dependence of $[Fe(II)EDTA]^{2-}$ Mims NK-ENDOR spectra collected at $B_0 = 45$ G. Other conditions are as in Fig. 3B. When $\tau < 320$ ns, the separation of the two ENDOR lines is independent of τ. However, beyond this point it decreases with increasing τ. See text for discussion.

CONCLUSIONS

A joint ESEEM and ENDOR study of the non-Kramers, $S = 2$ ferrous ion of $[Fe(II)EDTA]^{2-}$ has disclosed an anomalous equivalence of the experimental patterns produced by the two techniques. A simple theoretical treatment of the frequency-domain patterns expected for NK-ESEEM and NK-ENDOR rationalizes this correspondence and further suggests that the very observation of NK-ENDOR is the result of an unprecedentedly large hyperfine enhancement effect. Analysis of the NK-ESEEM measurements yields the quadrupole parameters for the ^{14}N ligands of $[Fe(II)EDTA]^{2-}$, $K = 1.16(1)$ MHz, $0 \leq \eta \leq 0.05$, which have been interpreted in terms of bonding parameters with the Townes–Dailey model, and indicates that the electronic zero-field splitting tetragonal axis lies along the N–N (u) direction indicated in Fig. 6. The theoretical considerations have further disclosed a lacuna in our understanding of the Mims NK-ENDOR phenomenon, and this will be the subject of a later report.

ACKNOWLEDGMENTS

We gratefully acknowledge the superb technical support of Mr. Clark E. Davoust. This work has been supported by the NSF (MCB 9507061) and NIH (HL 13531).

REFERENCES

1. B. Bleaney and H. E. D. Scovil, *Phil. Mag.* **43,** 999–1000 (1952).
2. M. Tinkham, *Proc. R. Soc. London A* **236,** 535–548 (1956).
3. J. M. Baker and B. Bleaney, *Proc. R. Soc. London A* **245,** 156–174 (1958).
4. M. P. Hendrich, E. Münck, B. G. Fox, and J. D. Lipscomb, *J. Am. Chem. Soc.* **112,** 5861–5865 (1990).
5. M. P. Hendrich and P. G. Debrunner, *Biophys. J.* **56,** 489–506 (1989).
6. B. M. Hoffman, B. E. Sturgeon, P. E. Doan, V. J. DeRose, K. E. Liu, and S. J. Lippard, *J. Am. Chem. Soc.* **116,** 6023–6024 (1994).
7. B. M. Hoffman, *J. Phys. Chem.* **98,** 11657–11665 (1994).
8. B. E. Sturgeon, P. E. Doan, K. E. Liu, D. Burdi, W. H. Tong, J. M. Nocek, N. Gupta, J. Stubbe, D. M. Kurtz, S. J. Lippard, and B. M. Hoffman, *J. Am. Chem. Soc.* **119,** 375–386 (1997).
9. T. Mizuta, J. Wang, and K. Miyoshi, *Bull. Chem. Soc. Jpn.* **66,** 2547–2551 (1993).
10. A. L. Feig and S. J. Lippard, *Chem. Rev.* **94,** 759–805 (1994).
11. B. J. Wallar and J. D. Lipscomb, *Chem. Rev.* **96,** 2625–2657 (1996).
12. C. Fan, P. E. Doan, C. E. Davoust, and B. M. Hoffman, *J. Magn. Reson.* **98,** 62–72 (1992).
13. W. B. Mims, *Phys. Rev. B* **5,** 2409–2419 (1972).
14. W. B. Mims, Electron Spin Echoes, *in* "Electron Paramagnetic Resonance" (S. Geschwind, Ed.), 263–351, Plenum Press, New York (1972).
15. M. K. Bowman and R. J. Massoth, Nuclear spin eigenvalues and eigenvectors in electron spin echo modulation, *in* "Electronic Magnetic Resonance of the Solid State" (J. A. Weil, Ed.), pp. 99–110, The Canadian Society for Chemistry, Ottawa (1987).
16. W. B. Mims, *J. Magn. Reson.* **59,** 291–306 (1984).
17. J. S. Griffith, *Phys. Rev.* **132,** 316–319 (1963).
18. G. M. Muha, *J. Magn. Reson.* **49,** 431–443 (1982).
19. N. M. Atherton, "Principles of Electron Spin Resonance." Physical Chemistry Series, Ellis Horwood, New York (1993).
20. E. Schempp and P. J. Bray, *in* "Physical Chemistry, an Advanced Treatise" (D. Henderson, Ed.), Chap. 11, Academic Press, New York, (1970).
21. J. E. Roberts, C. P. Cheng, and T. L. Brown, *J. Am. Chem. Soc.* **17,** 754–756 (1978).
22. E. A. C. Lucken, *in* "Nuclear Quadrupole Coupling Constants," pp. 217–247, Academic Press, New York (1969).
23. A. de Groot, R. Evelo, and A. J. Hoff, *J. Magn. Reson.* **66,** 331–343 (1986).
24. W. B. Mims, *Proc. R. Soc. London* **283,** 452–457 (1965).